

II–VI semiconductor alloy films: $\text{Cd}_{1-x}\text{Zn}_x\text{Te}$

P. GUPTA, K. K. CHATTOPADHYAY, S. CHAUDHURI, A. K. PAL
*Department of Materials Science, Indian Association for the Cultivation of Science,
 Calcutta 700 032, India*

Electrical conductivity and optical properties of undoped and copper-doped $\text{Cd}_{1-x}\text{Zn}_x\text{Te}$ ($0.1 < x < 0.8$) films prepared by the two-zone hot-wall technique, were measured at temperatures of 95–550 K. Copper-doped films showed an indirect transition at ~ 1.54 eV. It was observed that the grain-boundary scattering played an important role on the electron transport properties of the films. Increased doping dose culminated in segregation of dopant (copper) at the grain boundaries. The grains were partially depleted with filled traps and the trap states lay below the Fermi level.

1. Introduction

Polycrystalline thin films of $\text{Cd}_{1-x}\text{Zn}_x\text{Te}$ have been identified as one of the most promising materials for top cell applications in a two-cell tandem design [1]. In addition, $\text{Cd}_{1-x}\text{Zn}_x\text{Te}$ films are also being considered as an alternate substrate for growing HgCdTe films for infrared detectors [2]. However, little information is available on the above material in thin-film form [3–6]. Generally, a two-stage process [3, 4], two-zone evaporation [5] or MBE techniques [6] are applied for the preparation of films. The films, thus deposited, were generally characterized by measuring the optical properties with major emphasis towards the growth and process optimization of the films.

Studies on the electrical and optical properties of doped and undoped $\text{Cd}_{1-x}\text{Zn}_x\text{Te}$ films deposited by co-evaporating CdTe and ZnTe from a two-zone vertical evaporation source are presented here.

2. Experimental procedure

$\text{Cd}_{1-x}\text{Zn}_x\text{Te}$ films were deposited on to glass substrates by co-evaporating CdTe and ZnTe from two quartz crucibles placed inside a graphite heater. The details of the two-zone evaporation technique have been described elsewhere [5]. Doping of the films was done by co-evaporating copper from a concentric molybdenum boat during deposition. The compositions of the films were determined from EDX measurements and the optical transmittance, T_r , and reflectance, R , were recorded by Cary 2300 spectrophotometer. XRD traces were recorded by a Philips PW 1130 diffractometer. The films were deposited on to glass substrates at temperatures of 550 K and at a system pressure of $\sim 10^{-4}$ Pa.

3. Results and discussion

The electrical conductivity of doped and undoped films of $\text{Cd}_{1-x}\text{Zn}_x\text{Te}$ ($0.1 < x < 0.8$) was measured in the temperature range 95–550 K. Doping was done only in films having a band gap of ~ 1.7 eV which is

considered to be the optimum value for its use in highly efficient tandem solar cell structure. The films were predominantly p-type as determined from thermoelectric power measurements. XRD traces indicated the presence of a strong peak for $\langle 111 \rangle$ and the variation of lattice constant, a_0 , with x as determined from the XRD traces is shown in Fig. 1. For the sake of comparison we have also incorporated the values of a_0 obtained by Basol *et al.* [7] and Fontaine *et al.* [8] in Fig. 1 which showed a good agreement with the findings from this study. The variation of a_0 with x could be represented by the expression $a_0 = 6.503 - 0.399x$. This agrees well with the observation of Ringel *et al.* [9].

Fig. 2 shows transmission and scanning electron micrographs of the undoped and doped films. The scanning electron micrographs indicate rough surfaces for both the undoped (Fig. 2a) and doped (Fig. 2b) films. The transmission electron micrographs of $\text{Cd}_{1-x}\text{Zn}_x\text{Te}$ ($x \sim 0.63$) for films deposited on to NaCl (Fig. 2c) and glass (Fig. 2d) substrates indicate polycrystalline texture with cross-oriented grains. The films deposited on NaCl had larger grains with stronger orientation than that for films deposited on glass substrates.

Optical transitions were determined from the variation of absorption coefficient, α , with incident photon energy, $h\nu$, obtained from the transmittance–wavelength ($T_r-\lambda$) trace [10] and reflectance ($R-\lambda$)

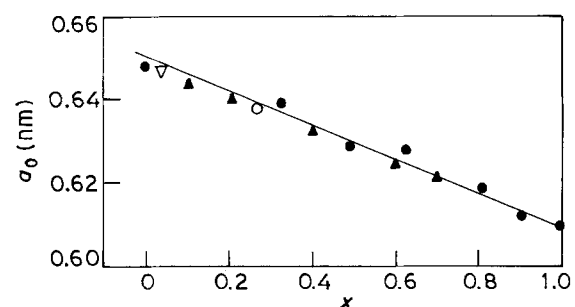


Figure 1 Variation of lattice constant, a_0 , with x . (●) Present work; (▲) [8]; (○) [6]; (△) [7]. (—) $a_0 = 6.503 - 0.399x$.

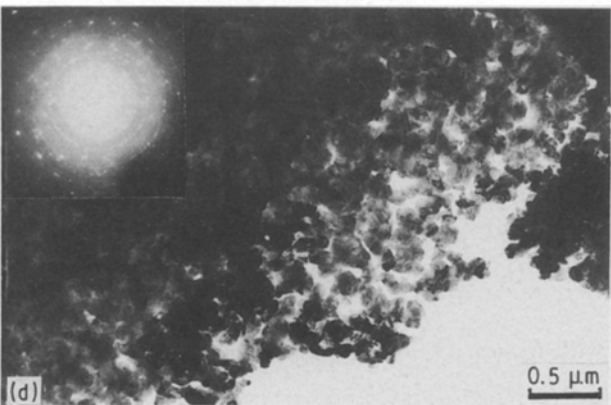
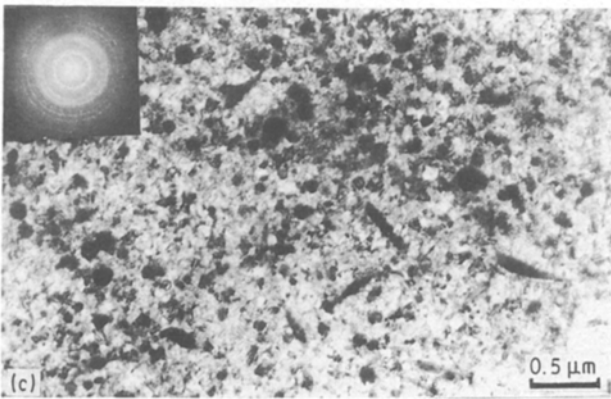
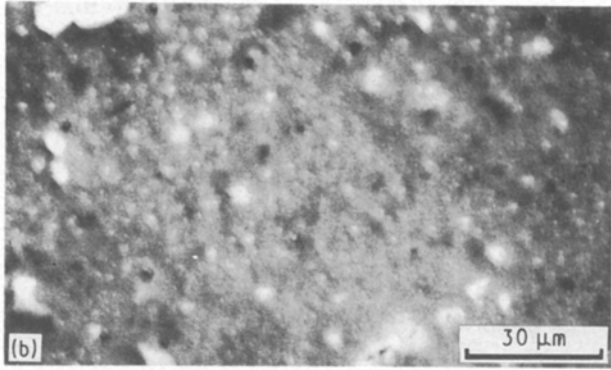
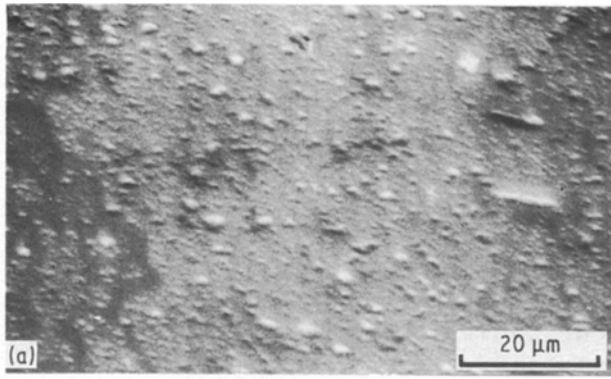


Figure 2 Scanning electron micrographs of (a) undoped and (b) doped, and transmission electron micrographs for undoped film deposited on (c) NaCl and (d) glass substrates for representative films.

trace [11]. The variation of band gap is similar to that reported in our earlier communication [5] with the exception that the doped films showed an additional allowed indirect transition at 1.54 eV, which is evident from the plots of $\ln \alpha$ versus $h\nu$ and $(\alpha h\nu)^{1/2}$ versus $h\nu$

as shown in the insets of Fig. 3. The variation of the refractive index with photon energy indicated a lowering of the refractive index with increasing doping dose.

The variation of conductivity, σ , with temperature for representative doped and undoped films is shown in Fig. 4. $\ln \sigma$ versus $1/T$ plots indicate two distinct domains at ~ 300 K. The electrical conductivity can be seen to increase sharply with temperature above ~ 300 K, while the change is appreciably slower at temperatures below it. The activation energies, E_{σ_1} and E_{σ_2} , were evaluated from the above plots and are shown in Table I. It can be observed (Fig. 5) that the activation energies, E_{σ_1} , of the films for the high-temperature domain showed a non-linear variation

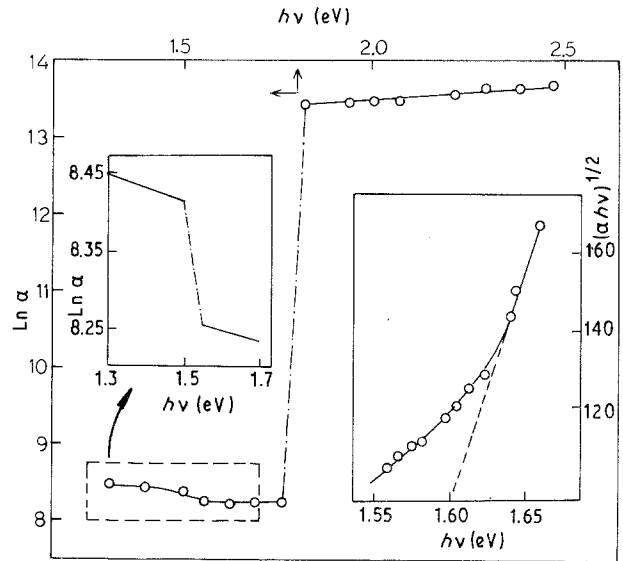


Figure 3 Variations of $\ln \alpha$ and $(\alpha h\nu)^{1/2}$ with $h\nu$.

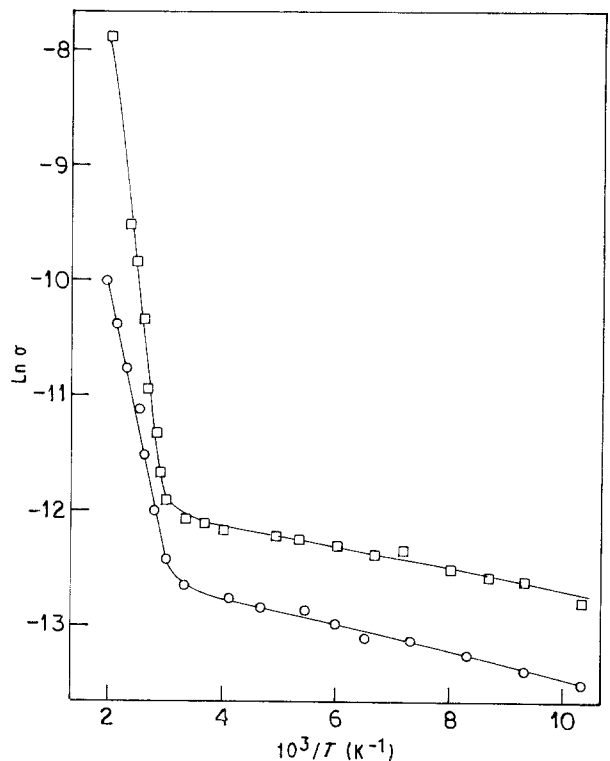


Figure 4 Plot of $\ln \sigma$ versus $1/T$ for two representative $\text{Cd}_{1-x}\text{Zn}_x\text{Te}$ films: (○) CZT-19 (undoped); (□) = CZT-24 (copper doped).

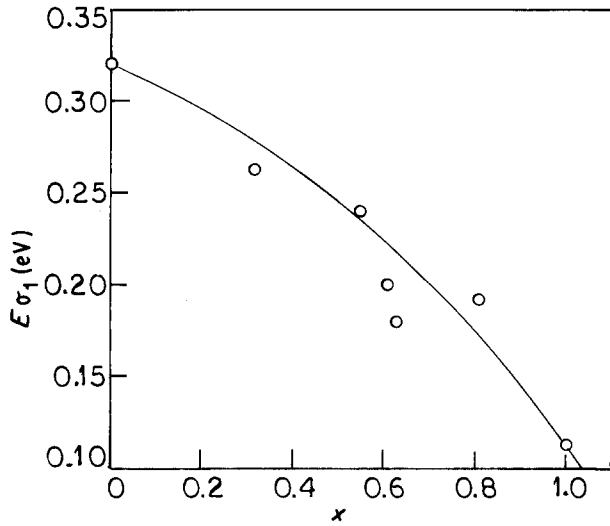


Figure 5 Variation of $E\sigma_1$ with x . (○) Experimental points; (—) theoretical plot with $b = 0.10$.

with x . This variation fitted well with the expression similar to that for band gaps [5, 12]

$$E\sigma_1(x) = E_2 + (E_1 - E_2 - b)x + bx^2 \quad (1)$$

where E_1 and E_2 are the activation energies of ZnTe and CdTe, respectively, and b the bowing parameter is given by [12]

$$b = \frac{Ze(r_1 + r_2)}{8\pi\epsilon_0} \left(\frac{1}{r_1} - \frac{1}{r_2} \right)^2 \times \exp \left[-s/2 \left(\frac{a^{3/2}}{4} \right) \right] \quad (2)$$

where Z is the valence number of interstitial ions, r_1 and r_2 are the Pauling covalent radii, a is the lattice constant for mid-composition of the alloy, s is the screening constant and ϵ_0 is the permittivity of free space. The best fit was obtained for $b = 0.10$ eV and it may be noted that this value is quite close to that (0.22 eV) obtained from theoretical considerations [12] with $r_1 = 0.148$ nm, $r_2 = 0.131$ nm, $s = 0.25$ and $\epsilon_0 = 8.85 \times 10^{-12}$ F m⁻¹.

Now, using Equation 1 and substituting the expression of activation energies in terms of resistivities, ρ , i.e. $kT \ln(\rho/\rho_0) = E\sigma$, we can obtain a relation

$$\ln(\rho_x/\rho_{0x}) = \ln(\rho_2/\rho_{02}) + [\ln(\rho_1/\rho_{01}) - \ln(\rho_2/\rho_{02}) - b/kT]x + bx^2/kT \quad (3)$$

so that

$$\ln \rho_x = \ln \rho_2 + [\ln \rho_1 - \ln \rho_2 - b/kT]x + bx^2/kT - \ln D \quad (4)$$

where D is a temperature-independent term and is given by

$$D = \rho_{0x}/[(\rho_{01}/\rho_{02})^x \rho_{02}] \quad (5)$$

ρ_{0x} , ρ_{01} and ρ_{02} are the pre-exponential terms corresponding to the resistivities ρ_x , ρ_1 and ρ_2 of Cd_{1-x}Zn_xTe, ZnTe and CdTe, respectively. It may be noted that for all practical purpose $D \approx 1$.

Fig. 6 shows the variation of $\ln \rho$ with x and it can be observed that this variation is similar to that observed for $E\sigma_1$. The above experimental behaviour can well be described by Equation 3 with $b \approx 0.07$ eV.

Polycrystalline films are generally characterized by the presence of moderately large grains which are often comparable with the mean free path of the charge carriers and grain-boundary scattering then becomes a predominant factor controlling the electron transport properties in those films. Applying the grain-boundary theory [13] as modified by Baccarani *et al.* [14], the electrical conductivity, σ , can be expressed in two forms:

(a) when the crystallites are fully depleted of carriers

$$\sigma = \left(\frac{e^2 L N_a}{Q_t - L N_a} \right) \left(\frac{2\pi m^* kT}{h^3} \right) \exp(-E_\alpha/kT) \quad (6)$$

where e is the electronic charge, L is the grain size, N_a is the carrier concentration, Q_t is the density of trap states at the grain boundary, m^* is the effective mass of the charge carrier and E_α is the activation energy of the acceptor level;

(b) when the grains are partially depleted, we may have two cases

(i) $E_f - (E_t + E_b) \gg kT$; i.e. the traps with energy E_t are filled

$$\sigma = \frac{e^2 L n_0}{(2\pi m^* kT)^{1/2}} \exp(-E_\alpha/kT) \quad (7)$$

with $E_\alpha = E_b$, E_b being the barrier height at the grain boundary;

(ii) $(E_t + E_b) - E_f \gg kT$; i.e. traps are partially filled

$$\sigma = \frac{4eL}{Q_t h^6} (2\pi m^* kT)^{5/2} \left(\frac{2\epsilon E_b}{N_a} \right)^{1/2} \exp(-E_\alpha/kT) \quad (8)$$

with $E_\alpha = E_g/2 - E_t$, E_g being the band gap.

TABLE I Values of $E\sigma_1$, $E\sigma_2$, E_b , Q_t and $E_f - E_t$ for different Cd_{1-x}Zn_xTe films

Film	x	$E\sigma_1$ (eV)	$E\sigma_2$ (meV)	E_b (meV)	Q_t (10 ¹⁰ cm ⁻²)	$E_f - E_t$ (meV)
CZT-14 ^a	0.32	0.26	2.41	2.0	6.98	-5.0
CZT-18 ^a	0.55	0.24	3.0	11.0	6.98	-6.0
CDT-19 ^a	0.61	0.20	17.0	16.4	8.15	-0.93
CZT-23 ^a	0.63	0.18	5.0	13.0	7.3	-4.0
CZT-24 (doped)	0.65	0.37	8.0	14.0	7.5	-3.0

^a Undoped films.

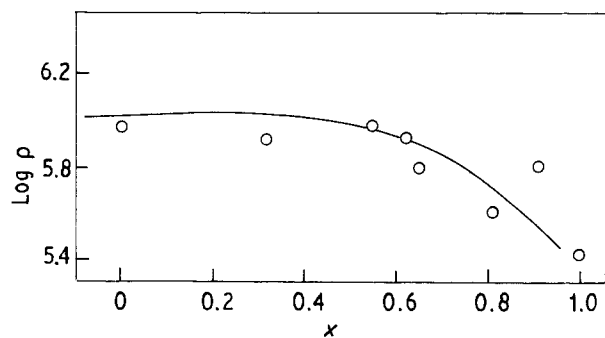


Figure 6 Variation of $\log \rho$ with x for $\text{Cd}_{1-x}\text{Zn}_x\text{Te}$ films. (○) Experimental points; (—) theoretical plot with $b = 0.07$.

It was observed that the experimental data fitted extremely well with Equation 7 for the entire temperature range below 300 K as can be seen from the $\ln(\sigma T^{1/2})$ versus $1/T$ plot (Fig. 7). This suggests that the grains are partially depleted with completely filled traps. The values of E_b can be obtained from the slopes of the above plots ($T < 300$ K), and are given in Table I. The density of trap states, Q_t , can be computed by using the relation [13]

$$E_b = (e^2 Q_t^2) / (8\epsilon N_a) \quad (9)$$

where ϵ is the dielectric constant. The values of Q_t obtained by using N_a values ($\sim 10^{15} \text{ cm}^{-3}$) obtained from the capacitance-voltage measurements, are shown in Table I. The position of the trap levels, E_t , with respect to the Fermi level, E_f , was obtained from the above model [14] and are shown in Table I. It may be observed that neither the barrier height, E_b , nor the density of trap states, Q_t , showed any significant change with doping doses. The location of the trap states E_t was around $\sim 1\text{--}6$ meV below the Fermi level. It may be noted here that the experimental data showed an extremely poor fit with Equation 8 as

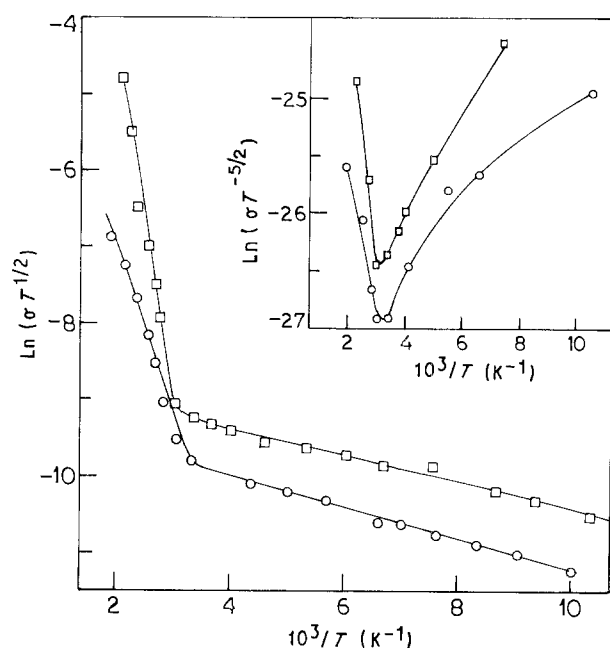


Figure 7 Plot of $\ln(\sigma T^{1/2})$ versus $1/T$ for two representative films: (○) CZT-19 (undoped); (□) CZT-24 (copper doped). Inset shows the plot of $\ln(\sigma T^{-5/2})$ versus $1/T$.

shown by the plot of $\ln(\sigma T^{-5/2})$ versus $1/T$ (inset, Fig. 7).

The change in σ with copper doping needs careful control of addition and dispersion of copper in $\text{Cd}_{1-x}\text{Zn}_x\text{Te}$ films. The conductivity did not change significantly with doping density. But the temperature dependence of conductivity of the doped films showed an interesting behaviour. Increase in doping density culminated in a negative temperature coefficient of conductivity which indicated that the copper becomes segregated at the grain boundaries. This segregation will lead towards a very low resistive (i.e. near metallic) grain boundaries which would cause a negative temperature coefficient of conductivity. It may be noted that the band gap of the material did not change with increase in doping density but had a predominant effect on the indirect transition in the doped films. The indirect transitions became more significant with increased doping which were reflected in a sharper fall of $\ln \alpha$ at the corresponding band edge at energies higher than that for films with lower doping density. Annealing in nitrogen at ~ 650 K tends to disperse the segregated copper dopants through grain-boundary diffusion and the films then indicate an indirect transition at ~ 1.54 eV. However, the temperature coefficient of conductivity did not show any significant change with the above annealing process.

From the above analyses it is clear that for $\text{Cd}_{1-x}\text{Zn}_x\text{Te}$ films, the electrical conductivity is mainly controlled by the grain-boundary scattering processes with partially depleted grains and filled traps. The trap states lie at energies $\sim 1\text{--}6$ meV below the Fermi level with E_b values $\sim 0.012\text{--}0.036$ eV. This means that at temperatures below ~ 300 K, the carriers will be trapped in the trap states before being conducted to the valence band at higher temperatures. The high temperature conductivity is generally governed by the exponential terms contained in the expressions given in Equations 5–8. Because the exponential term dominates at higher temperatures, the experimental data will show a reasonably good fit with any of the above equations at temperatures > 300 K.

Acknowledgements

Two of the authors (P. G. and K. K. C.) gratefully acknowledge the financial help offered to them by the C.S.I.R., Government of India, during the course of this work. The authors thank Dr S. K. Bhattacharyya, C.G.C.R.I., Calcutta, for his help in recording the optical traces.

References

1. J. C. C. FAN and B. J. PALM, *Solar Cells* **12** (1984) 401.
2. J. S. GOELA and R. L. TAYLOR, *Appl. Phys. Lett.* **51** (1987) 928.
3. A. ROHATGI, S. A. RINGEL and S. SUDHARSANAN, *Solar Cells* **27** (1989) 219.
4. B. M. BASOL and V. K. KAPUR, *ibid.* **30** (1991) 143.
5. K. K. CHATTOPADHYAY, A. SARKAR, S. CHAUDHURI and A. K. PAL, *Vacuum* **42** (1991) 1113.

6. A. ROHATGI, R. SUDHARSANAN, S. A. RINGEL and M. H. MacDOUGEL, *Solar Cells* **30** (1991) 109.
7. B. M. BASOL, V. K. KAPUR and R. C. KULLBERG, in "Proceedings of the 20th IEEE Photovoltaic Specialists Conference", Las Vegas, NV (1988) p. 1500.
8. C. FONTAINE, J. P. GAILLIARD, S. MAGLI, A. MILLION and J. PIAQUET, *Appl. Phys. Lett.* **50** (1987) 903.
9. S. A. RINGEL, R. SUDHARSANAN, A. ROHATGI and W. B. CARTER, *J. Electronic Mater.* **19** (1990) 259.
10. J. C. MANIFACIER, M. de MURCIA, J. P. FILLARD and E. VICARIO, *Thin Solid Films* **41** (1977) 127.
11. D. BHATTACHARYYA, S. CHAUDHURI and A. K. PAL, *Vacuum*, **43** (1992) 313.
12. R. HILL, *J. Phys. C Solid State Phys.* **7** (1974) 521.
13. J. Y. W. SETO, *J. Appl. Phys.* **46** (1975) 5247.
14. G. BACCARANI, B. RICCO and G. SPADINI, *ibid.* **49** (1978) 5565.

*Received 2 December 1991
and accepted 7 April 1992*